Letter | Editors' Suggestion

Quantum criticality and entanglement for the two-dimensional long-range Heisenberg bilayer

Menghan Song,[1] Jiarui Zhao,[1,*] Yang Qi,[2,3,4] Junchen Rong,[5,†] and Zi Yang Meng[1,‡]

[1]*Department of Physics and HKU-UCAS Joint Institute of Theoretical and Computational Physics, The University of Hong Kong, Pokfulam Road, Hong Kong SAR, China*

[2]*State Key Laboratory of Surface Physics, Fudan University, Shanghai 200438, China*

[3]*Center for Field Theory and Particle Physics, Department of Physics, Fudan University, Shanghai 200433, China*

[4]*Collaborative Innovation Center of Advanced Microstructures, Nanjing 210093, China*

[5]*Institut des Hautes Études Scientifiques, 91440 Bures-sur-Yvette, France*

(Received 12 June 2023; revised 14 December 2023; accepted 7 February 2024; published 26 February 2024)

The study of quantum criticality and entanglement in systems with long-range (LR) interactions is still in its early stages, with many open questions remaining to be explored. In this work, we investigate critical exponents and scaling of entanglement entropy (EE) in the LR bilayer Heisenberg model using large-scale quantum Monte Carlo simulations. By applying modified (standard) finite-size scaling above (below) the upper critical dimension and field theory analysis, we obtain precise critical exponents in three regimes: the LR Gaussian regime with a Gaussian fixed point, the short-range (SR) regime with Wilson-Fisher exponents, and a LR non-Gaussian regime where the critical exponents vary continuously from LR Gaussian to SR values. We compute the Rényi EE both along the critical line and in the Néel phase, and we observe that as the LR interaction is enhanced, the area-law contribution in EE gradually vanishes both at quantum critical points (QCPs) and in the Néel phase. The log-correction in EE arising from sharp corners at the QCPs also decays to zero as the LR interaction grows, whereas that for Néel states, caused by the interplay of Goldstone modes and restoration of the symmetry in a finite system, is enhanced. Relevant experimental settings to detect these nontrivial properties for quantum many-body systems with LR interactions are discussed.

DOI: 10.1103/PhysRevB.109.L081114

Introduction. In recent years, research on long-range (LR) interacting quantum many-body systems has attracted significant attention from the perspectives of statistical physics, renormalization group field theory, and lattice model computation. These systems exhibit many exotic properties that await to be explored thoroughly, such as the modification of dynamic spectra [1–5], the violation of area-law scaling of entanglement entropy (EE) [6,7], and the breaking of the Lieb-Robinson bound [8–10]. Moreover, with the experimental realizations of quantum many-body systems with LR interactions, such as the Rydberg atom arrays [11–15] and programmable quantum simulators [16–21], and the magic-angle twisted bilayer graphene and two-dimensional (2D) moiré materials [22–73], there grows significant motivation to examine the novel properties of such systems.

In the meantime, the exploration of entanglement properties, predominantly the scaling behavior of entanglement entropies, has emerged as a pivotal subject within the field of condensed-matter physics. Such a focus derives from its capacity to effectively characterize various quantum states of matter, as well as the transitions between them, including those beyond the conventional Landau-Ginsburg-Wilson paradigm. Preceding investigations of EE have mainly concentrated on short-range (SR) systems [74–78]. When considering long-range systems, intriguing results have been found, including the violation of area-law scaling in one dimension (1D) [6,7], the upper bound of area-law coefficient [79], and so on. The unbiased scaling behavior of EE including subleading corrections in 2D long-range systems, however, has yet to be explored, primarily due to computational limitations. Nevertheless, the advent of nonequilibrium methods for measuring Rényi entanglement entropies [80–84] has opened new avenues for research. These advancements have made the precise detection of such properties in 2D long-range systems increasingly feasible.

In this Letter we examine both the entanglement and the critical properties for such systems in two dimensions by studying the LR spin-1/2 antiferromagnetic bilayer Heisenberg model with intralayer power-law decaying ($\frac{1}{r_{ij}^{\alpha}}$) interactions. For the SR case with only nearest-neighbor couplings, the system has an $SU(2)$ symmetry, and by tuning the ratio of inter- and intralayer couplings, the system undergoes a $(2+1)$-dimensional $O(3)$ continuous phase transition from the Néel state to a dimer product state [85,86]. With intralayer LR interactions, the systems still display the Néel-to-dimer phase transition; however, the transition is now modified. Here we aim to explore the critical and entanglement properties of this model systematically via field theory analysis, large-scale unbiased quantum Monte Carlo (QMC) simulations, and the nonequilibrium incremental algorithm for measuring EE [81–84,87–89].

Our findings reveal the critical exponents at the QCPs of the 2D LR bilayer Heisenberg model vary with α and can be

*jrzhao@connect.hku.hk
†junchenrong@gmail.com
‡zymeng@hku.hk

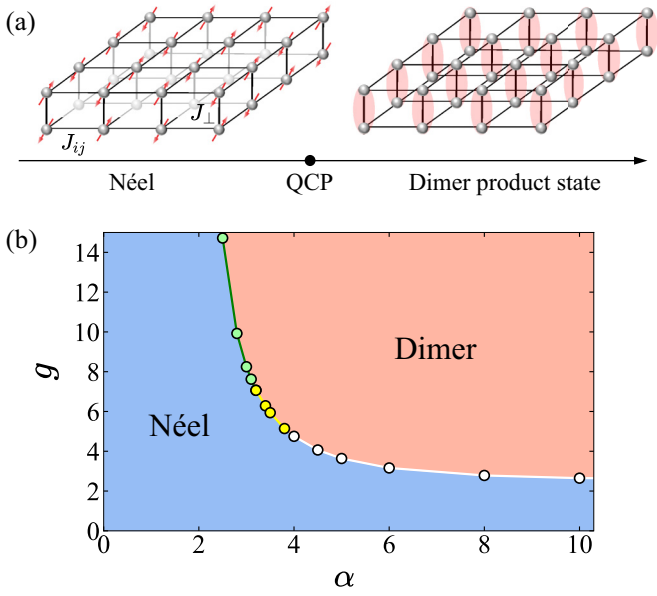

FIG. 1. Model and phase diagram of the 2D LR antiferromagnetic Heisenberg bilayer. (a) The bilayer antiferromagnetic model with interlayer interaction $J_\perp$ and intralayer LR interaction J_{ij}. (b) The ground-state phase diagram of the model expanded by the axes of α and $g = \frac{J_\perp}{J}$, obtained from QMC simulation and finite-size analysis, as exemplified in Figs. 2(a) and 2(b) and in the Supplemental Material [90]. The Néel phase spontaneously breaks the spin $SU(2)$ symmetry and the dimer phase is a product state without symmetry breaking. The QCPs separating them belong to the $(2+1)$D $O(3)$ universality when $\alpha > \alpha_c = 3.9621$, a non-Gaussian fixed point when $\frac{10}{3} < \alpha < \alpha_c$, and a Gaussian fixed point when $\alpha < \frac{10}{3}$. QCPs in LR Gaussian, LR non-Gaussian, and SR regions are denoted by green, yellow, and white dots (where the simulations are performed) and lines, respectively.

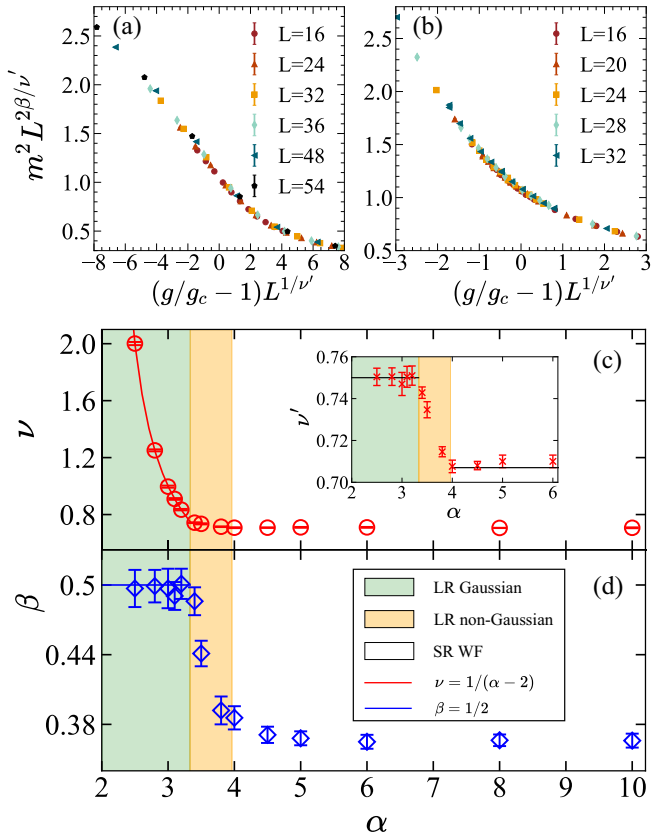

FIG. 2. Data collapse and the critical exponents ν and β obtained in $\alpha \in (2, 10]$. (a) Data collapse at $\alpha = 8$ (SR case) with critical exponents $\nu = 0.706(1)$ and $\beta = 0.366(5)$. (b) Data collapse at $\alpha = 3$ (LR case with Gaussian fixed point above the upper critical dimension) with critical exponents $\nu' = 0.747(4)$, $\beta = 0.497(7)$, and $\nu = \nu' \frac{d}{d_{\rm uc}} = 0.996(7)$. The green shaded area in panels (c) and (d) denote the LR Gaussian regime ($\alpha < \frac{10}{3}$) where $d = 2$ is larger than the upper critical dimension $d_{\rm uc}$. In the region of $\frac{10}{3} < \alpha < \alpha_c$ (yellow shaded area), the system is in a non-Gaussian fixed point, and when $\alpha > \alpha_c$ (white area) the critical exponents become their SR $(2+1)$D $O(3)$ WF values [86].

classified into three regimes: the LR regime ($\alpha < \frac{10}{3}$) with a Gaussian fixed point, the SR regime ($\alpha > \alpha_c$, with $\alpha_c = 3.9621$) with Wilson-Fisher (WF) critical exponents, and a LR non-Gaussian regime ($\frac{10}{3} < \alpha < \alpha_c$) where critical exponents vary continuously from the LR to SR regimes. In addition, we find that both the area-law and the corner correction coefficients of EE at the critical points decrease as LR interactions become stronger. However, in the Néel state, only the area-law coefficient decays as α becomes smaller, and the logarithmic corrections increase as α decreases, attributing to the variation of the anomalous dynamical exponent $z(\alpha)$ as a function of α [1,2].

Model and method. We consider the spin-1/2 Heisenberg model on a square-lattice bilayer with antiferromagnetic LR intralayer coupling J_{ij} and interlayer coupling $J_\perp$ with periodic boundary conditions, as shown in Fig. 1(a). The Hamiltonian is

$$H = \sum_{i \neq j} J_{ij}(\mathbf{S}_{i,1} \cdot \mathbf{S}_{j,1} + \mathbf{S}_{i,2} \cdot \mathbf{S}_{j,2}) + J_\perp \sum_i \mathbf{S}_{i,1} \cdot \mathbf{S}_{i,2}, \quad (1)$$

where $J_{ij} = J \frac{(-1)^{|x_i+y_i-x_j-y_j+1|}}{|\mathbf{r}_i - \mathbf{r}_j|^\alpha}$ is defined as a staggered coupling parameter which introduces no frustrations, and subscripts 1 and 2 denote different layers. We denote $g = J_\perp/J$ as the tuning parameter and previous studies have shown that, when there are only nearest-neighbor intralayer interactions, $g_c = 2.5220(1)$ separates the Néel-ordered phase with the dimer product phase and this transition is in the $(2+1)$D $O(3)$ universality class [85,86]. We consider the Ewald-modified coupling parameter [91–94] in the form of $\tilde{J}_{ij} = \sum_{m,n=-\infty}^{\infty} \frac{(-1)^{|x_i+y_i-x_j-y_j+1|}}{|\mathbf{r}_i - \mathbf{r}_j + mL_x\mathbf{e}_x + nL_y\mathbf{e}_y|^\alpha}$ to tackle the strong finite-size effect in the LR Gaussian regions. In practice we truncate the summation at $m, n = \pm 500$, which is sufficient to obtain a good finite-size scaling (FSS) behavior as exemplified in Figs. 2(a) and 2(b). At larger α, we find the original coupling J_{ij} can also obtain converged results.

We also notice that the FSS forms should be modified when the system enters the LR Gaussian region where the system's spatial dimension d is greater than the upper critical dimension $d_{\rm uc}$. In our case, as is discussed in the field theory analysis section, $d_{\rm uc} = \frac{3}{2}(\alpha - d)$ and the system thus enters the LR Gaussian regime when $\alpha < \frac{10}{3}$. Therefore, we write the scaling function that unifies both cases in data collapse to

extract the critical exponents ν and β as [92–100]

$$m^2 \sim L^{-2\beta/\nu'} f[L^{1/\nu'}(g-g_c)], \quad g \sim g_c, \tag{2}$$

with $\nu' = \begin{cases} \nu & \text{for } d < d_{\rm uc} \\ \nu \frac{d_{\rm uc}}{d} & \text{for } d > d_{\rm uc}. \end{cases}$ Here $\langle m^2 \rangle$ is the square of the Néel order parameter $m = \frac{1}{N}\sum_{\mathbf{r}} (-1)^{r_x+r_y} S^z_{\mathbf{r}}$ and ν is the actual correlation length exponent. The phase transition point g_c can be located by crossing points of Binder ratios $U(g,L) = \frac{5}{2}(1 - \frac{1}{3}\frac{\langle m^4 \rangle}{\langle m^2 \rangle^2})$ for various system sizes. The scaling of the Binder ratio crossing points follows the relation of $g^*(L) = aL^{-b} + g_c$. In practice, we set g_c, ν', and β as free parameters and adapt a stochastic data collapse scheme to determine their values accurately [18,90,101]. Representative results are shown in Figs. 2(a) and 2(b). We have simulated linear system sizes up to $L = 54$ in the SR regime and up to $L = 32$ in the LR regime, with the inverse temperature $\beta = L$.

Field theory analysis. To analyze the QCPs, we consider the following quantum field theory,

$$S = S_G + S_{\rm int}, \tag{3}$$

with the Gaussian term $S_G = \int d\tau dx^d [\sum_i \partial_\tau \phi^i(x,\tau)]^2 + \int d\tau dx^d dx'^d \frac{\sum_i \phi^i(x,\tau)\phi^i(x',\tau)}{|x-x'|^{d+\sigma}}$ and the interaction term $S_{int} = \lambda \int d\tau dx^d \{\sum_i [\phi^i(x,\tau)]^2\}^2$. It is well know that the $(2+1)$D short-range bilayer antiferromagnetic model is in the classical three-dimensional Heisenberg universality class [102]. By universality, the model and the field theory written in Eq. (3) (with the second term in Eq. (3) replaced by the corresponding local term $\int dx^d dt [\nabla \phi^i(x)]^2$) share the same critical behavior. In particular, the scalar field (ϕ^1, ϕ^2, ϕ^3) can be identified as the expectation value of the three-component vector $\langle \mathbf{S} \rangle$. To describe the long-range model, one should instead include the nonlocal spatial interaction term in Eq. (1). To match the lattice model, we set $\alpha = d + \sigma$. Under the scaling transformation $\tau \to s^z \tau$, $x \to sx$, and $\phi^i \to s^{-\Delta_\phi}\phi^i$, the Gaussian action S_G remains invariant if we choose $z^G = \frac{\alpha - d}{2}$ and $\Delta^G_\phi = \frac{3d-\alpha}{4}$. After fixing z and Δ_ϕ, the coupling constant transforms as

$$\lambda \to s^{\frac{1}{2}(3\alpha - 5d)}\lambda. \tag{4}$$

When $\alpha < \frac{5d}{3}$, the ϕ^4 term is irrelevant, the Gaussian fixed point is stable. When $\alpha > \frac{5d}{3}$, the ϕ^4 term is relevant, which triggers renormalization group flow towards an infrared (IR) fixed point. For a fixed σ, we define the upper critical dimension to be $d_{uc} = \frac{3}{2}\sigma$. At this IR fixed point, the dynamical critical exponents $z^{\rm IR}(\alpha)$ and the scaling dimension $\Delta^{\rm IR}_\phi(\alpha)$ will be renormalized. They clearly depends on α, even though the precise form of the dependence is not known. This, in principle, can be studied using quantum field theory techniques by treating $\epsilon = \alpha - \frac{5d}{3}$ as the perturbation parameter (a similar study of the finite-temperature LR model was famously done in Ref. [103]). We expect at some α_c, the critical point of the LR models becomes equivalent to the $(2+1)$D SR Heisenberg model. This will be confirmed by our numerical study later. The crossover from LR to SR happens when $z^{\rm IR}(\alpha) = 1$.

We now focus on the $d = 2$ case. To calculate α_c, we need to consider perturbation around the SR model. That is, we consider the following action [104]:

$$S = S_{\rm CFT}[\hat{\phi}^i(x)] + \int d\tau dx^2 dx'^2 \frac{\sum_i \hat{\phi}^i(x,\tau)\hat{\phi}^i(x',\tau)}{|x-x'|^\alpha}. \tag{5}$$

Here $S_{\rm CFT}$ formally denotes the action of the SR model at criticality, which corresponds to a conformal field theory (CFT). This CFT has been well studied. In particular, the CFT action has a scaling symmetry with $(t,x) \to (st, sx)$. Also, under this system, the scalar field transforms as $s^{-\Delta_\phi}\hat{\phi}(st, tx)$, with scaling dimension $\Delta_\phi \approx 0.518\,92$ [105]. The LR term is relevant when $\alpha < \alpha_c = 3.9621$. The $\alpha = 4$ model is another special point. When $\alpha = 4$, the action Eq. (3) is precisely the SR action after Fourier transformation. The point is, therefore, in the SR region, which is consistent with $\alpha_c = 3.9621$.

Critical behavior. We first use the crossing points of Binder ratios $g^*(L)$ to locate g_c by fitting to the relation $g^*(L) = aL^{-b} + g_c$. Then we set g_c as a free value around the fitted value and perform data collapse to determine the values of g_c, ν', and β according to Eq. (2), and the results are exemplified in Figs. 2(a) and 2(b) for the cases of $\alpha = 3$ and 8. We employ the stochastic data-collapse approach to obtain high-accuracy exponents; the detailed description and examples are given in the Supplemental Material [90]. The value of ν can then be calculated from the relation $\nu' = \frac{d_{\rm uc}}{d}\nu$. Note that the expected value of ν in the LR Gaussian regime is $\nu = \frac{1}{\alpha - d}$ and $d_{\rm uc} = \frac{3}{2}(\alpha - d)$, so ν' will take the value of 0.75 in the entire Gaussian regime.

We then plot the obtained critical exponents ν and β versus the interaction exponent α. As shown in Figs. 2(c) and 2(d), when $\alpha > \alpha_c$ the critical exponents take the SR values of the $(2+1)$D $O(3)$ universality class with $\nu = 0.706(1)$ and $\beta = 0.366(5)$ [85,86]. When $\alpha < \frac{10}{3}$, the system enters the LR Gaussian regime with $\nu = \frac{1}{\alpha - 2}$ and $\beta = 0.5$. Between these two regimes, the critical exponents ν and β vary continuously with α from the SR to the LR values. The deviation of β from its SR value at $\alpha = 4$ is due to strong finite-size effects near the crossover at $\alpha = \alpha_c$.

Entanglement entropy. The violation of area-law scaling of EE in 1D quantum spin chains with LR interactions has been observed via density matrix renormalization group (DMRG) [6,7]. However, apart from a few works [79,106] discussing the reliability of area-law scaling of EE in LR systems, the important scaling form of EE for 2D LR systems is unexplored. Meanwhile, with the fast development of QMC algorithms for EE computation [81–84,87,88,107], the Rényi EE now can be measured with high precision and efficiency both in phases and at the critical points in 2D systems. For 2D SR systems, EE takes the form of

$$S(l) = al - s_c \ln l + c, \tag{6}$$

where l is the length of the entanglement boundary and the logarithmic term arises from the contribution of sharp corners on the boundary. For SR models, the value of s_c is universal and $s_c \approx 0.081$ for four $\frac{\pi}{2}$ corners at the $(2+1)$D $O(3)$ criticality [78,82,83]. However, for LR systems the scaling forms of EE have not been explored, especially at their QCPs. We measure the second Rényi EE $S^{(2)}_A$ at the QCPs in Fig. 1(b). We choose a $\frac{L}{2} \times \frac{L}{2}$ square region as A as shown in the inset of Fig. 3(a) and use the scaling relation defined in Eq. (6) to fit our results. The fitting results are shown in Figs. 3(b) and 3(c), and one finds as α decreases the area-law coefficient gradually decays to a small value, which indicates that quantum entanglement at the criticality becomes weaker

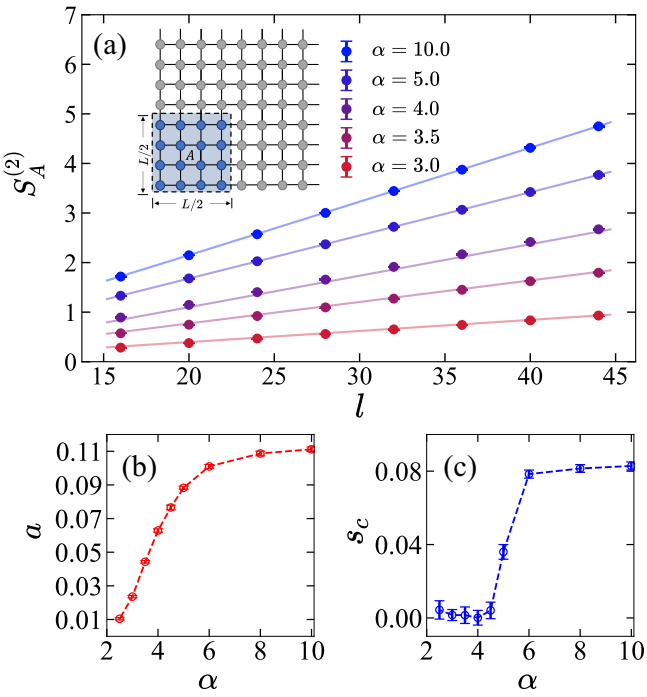

FIG. 3. EE at the QCPs. $S_A^{(2)}$ and its scaling behavior at the QCPs shown in Fig. 1(b) with system sizes $L = 8, 10, 12, \ldots, 22$. (a) Rényi entropies versus the system sizes for different interaction powers α. The inset shows the square entanglement region A with the boundary length $l = 2L$. (b) The area-law coefficient a versus α. (c) The log-coefficient s_c versus α.

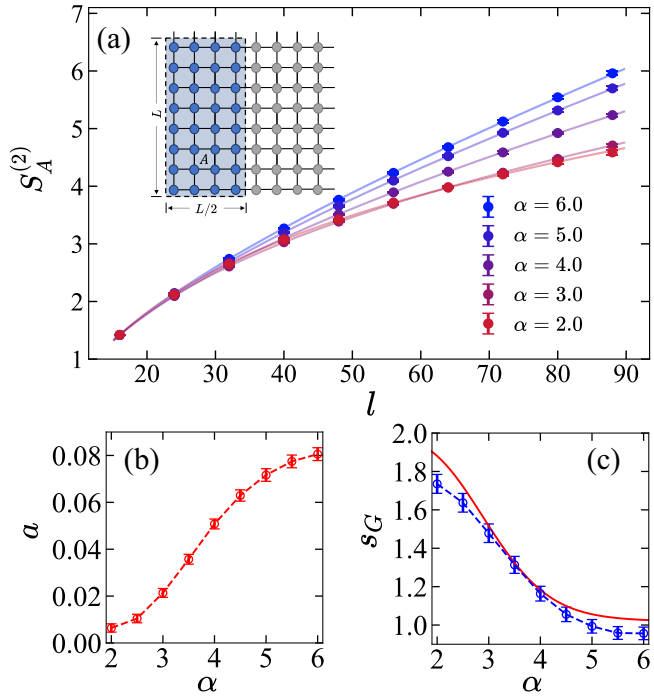

FIG. 4. EE inside the Néel phase. $S_A^{(2)}$ and its scaling behavior for the single-layer LR Heisenberg model, i.e., $g = 0$ in Eq. (1) in the Néel phase with system sizes $L = 8, 12, 16, \ldots, 44$. (a) Rényi entropies versus the system sizes for different interaction powers α. The inset shows the cylinder entanglement region A with the boundary length $l = 2L$. For clarity, $S_A^{(2)}$ is modified with a constant so that $S_A^{(2)}$ ($l = 16$) is the same for every α. (b) The area-law coefficient a versus α. (c) The logarithmic coefficient s_G versus α. The red line shows the result $s_G = \frac{N_G[d-z(\alpha)]}{2}$, with $z(\alpha)$ obtained from spin wave theory and QMC data ($L = 64$) in Ref. [2].

when the interactions becomes more long-ranged. This can be understood by the fact that the critical points are described by a LR Gaussian theory for $\alpha < \frac{10}{3}$ and the system becomes more mean-field-like when LR interactions are enhanced. The corner corrections drop rapidly to zero as the system goes into the LR region $\alpha < \alpha_c$, which can be understood as strong LR interactions trivializing the geometry of sharp corners and making the EE less sensitive to the shape of the entanglement boundary.

We also examine the scaling of EE in the Néel phase in Fig. 4. As shown in the inset of Fig. 4(a), we choose region A to be the $L \times \frac{L}{2}$ partition with a smooth boundary. In this setting, the logarithmic corrections are purely from the interplay between gapless Goldstone modes and restoration of the symmetry in a finite system [5,76]. With the addition of power-law decaying LR interactions, the dynamic exponent $z(\alpha)$ of the Néel state is modified [1,2] as well as the structure of tower of state [5,76]. In this case, the s_c in Eq. (6) needs to be replaced by $-s_G = -\frac{N_G[d-z(\alpha)]}{2}$ and N_G is the number of Goldstone modes. We thus fit our results of EE with Eq. (6) and the fitting results are shown in Figs. 4(b) and 4(c). We find the area-law coefficient a also decays as the LR interactions get stronger, whereas the logarithmic coefficient s_G increases from the SR value $s_G = \frac{N_G}{2} = 1$ to $s_G \approx 1.76$ as α decreases from 6 to 2. We substitute the data of $z(\alpha)$ from previous QMC and spin-wave analysis [2] into $s_G = \frac{N_G[d-z(\alpha)]}{2}$ and find good agreement with the fitted s_G, as shown in Fig. 4(c). The derivations in the SR and LR Gaussian regimes are attributed to finite-size effects.

Discussions. In this work, we address the important open questions regarding the critical exponents and scaling of EE in 2D LR quantum many-body systems. Through large-scale QMC simulations, we obtained precise critical exponents in the LR Gaussian regime with a Gaussian fixed point, the SR regime with WF exponents, and an LR non-Gaussian regime where the critical exponents vary continuously from LR to SR values. Our investigation of Rényi EE has revealed highly nontrivial features both along the QCP line and in the Néel phase, in that, as the interaction becomes longer-ranged, the area-law contribution in EE gradually vanishes, while the log-correction is enhanced in the Néel phase due to the anomalous dependence of the dynamical exponent $z(\alpha)$ on α. Our results have important implications for future theoretical and experimental investigations of LR interacting quantum many-body systems, including Rydberg atom arrays [11–15], programmable quantum simulators [16–19,21], and magic-angle twisted bilayer graphene and 2D moiré materials.

Acknowledgments. We thank S. Sachdev, F. Alet, F. Assaad, K. Sun, M. Scherer, S. Rychkov, L. Janssen, M. Cheng, and Y. Deng for valuable discussions on the related topic. M.H.S., J.R.Z., and Z.Y.M. acknowledge support from the Research Grants Council (RGC) of Hong Kong Special Administrative Region (SAR) of China (Projects No. 17301420, No. 17301721, No. AoE/P-701/20, No.

17309822, and No. HKU C7037-22G), the ANR/RGC Joint Research Scheme sponsored by the RGC of Hong Kong, SAR of China, and French National Research Agency (Project No. A_HKU703/22) and the HKU Seed Funding for Strategic Interdisciplinary Research "Many-Body Paradigm in Quantum Moiré Material Research." The work of J.R. is supported by the Huawei Young Talent program at the Institut des Hautes Études Scientifiques. The authors also acknowledge the Beijng PARATERA Tech CO., Ltd. [108], Tianhe-II platform at the National Supercomputer Center in Guangzhou, the HPC2021 system under the Information Technology Services, and the Blackbody HPC systemat the Department of Physics, University of Hong Kong for their technical support and generous allocation of CPU time.

[1] O. K. Diessel, S. Diehl, N. Defenu, A. Rosch, and A. Chiocchetta, Generalized Higgs mechanism in long-range-interacting quantum systems, Phys. Rev. Res. **5**, 033038 (2023).

[2] M. Song, J. Zhao, C. Zhou, and Z. Y. Meng, Dynamical properties of quantum many-body systems with long-range interactions, Phys. Rev. Res. **5**, 033046 (2023).

[3] E. Yusuf, A. Joshi, and K. Yang, Spin waves in antiferromagnetic spin chains with long-range interactions, Phys. Rev. B **69**, 144412 (2004).

[4] N. Defenu, T. Donner, T. Macrì, G. Pagano, S. Ruffo, and A. Trombettoni, Long-range interacting quantum systems, arXiv:2109.01063.

[5] I. Frérot, P. Naldesi, and T. Roscilde, Entanglement and fluctuations in the XXZ model with power-law interactions, Phys. Rev. B **95**, 245111 (2017).

[6] T. Koffel, M. Lewenstein, and L. Tagliacozzo, Entanglement entropy for the long-range Ising chain in a transverse field, Phys. Rev. Lett. **109**, 267203 (2012).

[7] Z. Li, S. Choudhury, and W. V. Liu, Long-range-ordered phase in a quantum Heisenberg chain with interactions beyond nearest neighbors, Phys. Rev. A **104**, 013303 (2021).

[8] L. Vanderstraeten, M. Van Damme, H. P. Büchler, and F. Verstraete, Quasiparticles in quantum spin chains with long-range interactions, Phys. Rev. Lett. **121**, 090603 (2018).

[9] M. C. Tran, A. Y. Guo, Y. Su, J. R. Garrison, Z. Eldredge, M. Foss-Feig, A. M. Childs, and A. V. Gorshkov, Locality and digital quantum simulation of power-law interactions, Phys. Rev. X **9**, 031006 (2019).

[10] L. Colmenarez and D. J. Luitz, Lieb-Robinson bounds and out-of-time order correlators in a long-range spin chain, Phys. Rev. Res. **2**, 043047 (2020).

[11] R. Samajdar, W. W. Ho, H. Pichler, M. D. Lukin, and S. Sachdev, Quantum phases of Rydberg atoms on a kagome lattice, Proc. Natl. Acad. Sci. USA **118**, e2015785118 (2021).

[12] Z. Yan, R. Samajdar, Y.-C. Wang, S. Sachedev, and Z. Y. Meng, Triangular lattice quantum dimer model with variable dimer density, Nat. Commun. **13**, 5799 (2022).

[13] G. Semeghini, H. Levine, A. Keesling, S. Ebadi, T. T. Wang, D. Bluvstein, R. Verresen, H. Pichler, M. Kalinowski, R. Samajdar, A. Omran, S. Sachdev, A. Vishwanath, M. Greiner, V. Vuletić, and M. D. Lukin, Probing topological spin liquids on a programmable quantum simulator, Science **374**, 1242 (2021).

[14] K. J. Satzinger, Y. J. Liu, A. Smith, C. Knapp, M. Newman, C. Jones, Z. Chen, C. Quintana, X. Mi, A. Dunsworth, C. Gidney, I. Aleiner, F. Arute, K. Arya, J. Atalaya, R. Babbush, J. C. Bardin, R. Barends, J. Basso, A. Bengtsson *et al.*, Realizing topologically ordered states on a quantum processor, Science **374**, 1237 (2021).

[15] Z. Yan, Y.-C. Wang, R. Samajdar, S. Sachdev, and Z. Y. Meng, Emergent glassy behavior in a kagome Rydberg atom array, Phys. Rev. Lett. **130**, 206501 (2023).

[16] R. Verresen, M. D. Lukin, and A. Vishwanath, Prediction of toric code topological order from rydberg blockade, Phys. Rev. X **11**, 031005 (2021).

[17] R. Samajdar, D. G. Joshi, Y. Teng, and S. Sachdev, Emergent $\mathbb{Z}_2$ gauge theories and topological excitations in Rydberg atom arrays, Phys. Rev. Lett. **130**, 043601 (2023).

[18] Z. Yan, X. Ran, Y.-C. Wang, R. Samajdar, J. Rong, S. Sachdev, Y. Qi, and Z. Y. Meng, Fully packed quantum loop model on the triangular lattice: Hidden vison plaquette phase and cubic phase transitions, arXiv:2205.04472.

[19] X. Ran, Z. Yan, Y.-C. Wang, J. Rong, Y. Qi, and Z. Y. Meng, Fully packed quantum loop model on the square lattice: Phase diagram and application for Rydberg atoms, Phys. Rev. B **107**, 125134 (2023).

[20] X. Ran, Z. Yan, Y.-C. Wang, J. Rong, Y. Qi, and Z. Y. Meng, Cubic* criticality emerging from quantum loop model on triangular lattice, arXiv:2309.05715.

[21] Y.-C. Wang, M. Cheng, W. Witczak-Krempa, and Z. Y. Meng, Fractionalized conductivity and emergent self-duality near topological phase transitions, Nat. Commun. **12**, 5347 (2021).

[22] G. Trambly de Laissardière, D. Mayou, and L. Magaud, Localization of Dirac electrons in rotated graphene bilayers, Nano Lett. **10**, 804 (2010).

[23] R. Bistritzer and A. H. MacDonald, Moiré bands in twisted double-layer graphene, Proc. Natl. Acad. Sci. USA **108**, 12233 (2011).

[24] J. M. B. Lopes dos Santos, N. M. R. Peres, and A. H. Castro Neto, Continuum model of the twisted graphene bilayer, Phys. Rev. B **86**, 155449 (2012).

[25] G. Trambly de Laissardière, D. Mayou, and L. Magaud, Numerical studies of confined states in rotated bilayers of graphene, Phys. Rev. B **86**, 125413 (2012).

[26] A. Rozhkov, A. Sboychakov, A. Rakhmanov, and F. Nori, Electronic properties of graphene-based bilayer systems, Phys. Rep. **648**, 1 (2016).

[27] Y. Cao, V. Fatemi, S. Fang, K. Watanabe, T. Taniguchi, E. Kaxiras, and P. Jarillo-Herrero, Unconventional superconductivity in magic-angle graphene superlattices, Nature (London) **556**, 43 (2018).

[28] Y. Cao, V. Fatemi, A. Demir, S. Fang, S. L. Tomarken, J. Y. Luo, J. D. Sanchez-Yamagishi, K. Watanabe, T. Taniguchi, E. Kaxiras *et al.*, Correlated insulator behaviour at half-filling in magic-angle graphene superlattices, Nature (London) **556**, 80 (2018).

[29] Y. Xie, B. Lian, B. Jäck, X. Liu, C.-L. Chiu, K. Watanabe, T. Taniguchi, B. A. Bernevig, and A. Yazdani, Spectroscopic signatures of many-body correlations in magic-angle twisted bilayer graphene, Nature (London) **572**, 101 (2019).

[30] X. Lu, P. Stepanov, W. Yang, M. Xie, M. A. Aamir, I. Das, C. Urgell, K. Watanabe, T. Taniguchi, G. Zhang *et al.*, Superconductors, orbital magnets and correlated states in magic-angle bilayer graphene, Nature (London) **574**, 653 (2019).

[31] A. Kerelsky, L. J. McGilly, D. M. Kennes, L. Xian, M. Yankowitz, S. Chen, K. Watanabe, T. Taniguchi, J. Hone, C. Dean *et al.*, Maximized electron interactions at the magic angle in twisted bilayer graphene, Nature (London) **572**, 95 (2019).

[32] Y. Da Liao, Z. Y. Meng, and X. Y. Xu, Valence bond orders at charge neutrality in a possible two-orbital extended hubbard model for twisted bilayer graphene, Phys. Rev. Lett. **123**, 157601 (2019).

[33] M. Yankowitz, S. Chen, H. Polshyn, Y. Zhang, K. Watanabe, T. Taniguchi, D. Graf, A. F. Young, and C. R. Dean, Tuning superconductivity in twisted bilayer graphene, Science **363**, 1059 (2019).

[34] S. L. Tomarken, Y. Cao, A. Demir, K. Watanabe, T. Taniguchi, P. Jarillo-Herrero, and R. C. Ashoori, Electronic compressibility of magic-angle graphene superlattices, Phys. Rev. Lett. **123**, 046601 (2019).

[35] Y. Cao, D. Chowdhury, D. Rodan-Legrain, O. Rubies-Bigorda, K. Watanabe, T. Taniguchi, T. Senthil, and P. Jarillo-Herrero, Strange metal in magic-angle graphene with near Planckian dissipation, Phys. Rev. Lett. **124**, 076801 (2020).

[36] C. Shen, Y. Chu, Q. Wu, N. Li, S. Wang, Y. Zhao, J. Tang, J. Liu, J. Tian, K. Watanabe, T. Taniguchi, R. Yang, Z. Y. Meng, D. Shi, O. V. Yazyev, and G. Zhang, Correlated states in twisted double bilayer graphene, Nat. Phys. **16**, 520 (2020).

[37] K. P. Nuckolls, M. Oh, D. Wong, B. Lian, K. Watanabe, T. Taniguchi, B. A. Bernevig, and A. Yazdani, Strongly correlated chern insulators in magic-angle twisted bilayer graphene, Nature (London) **588**, 610 (2020).

[38] T. Soejima, D. E. Parker, N. Bultinck, J. Hauschild, and M. P. Zaletel, Efficient simulation of Moiré materials using the density matrix renormalization group, Phys. Rev. B **102**, 205111 (2020).

[39] S. Chatterjee, M. Ippoliti, and M. P. Zaletel, Skyrmion superconductivity: DMRG evidence for a topological route to superconductivity, Phys. Rev. B **106**, 035421 (2022).

[40] E. Khalaf, N. Bultinck, A. Vishwanath, and M. P. Zaletel, Soft modes in magic angle twisted bilayer graphene, arXiv:2009.14827.

[41] M. Xie and A. H. MacDonald, Nature of the correlated insulator states in twisted bilayer graphene, Phys. Rev. Lett. **124**, 097601 (2020).

[42] E. Khalaf, S. Chatterjee, N. Bultinck, M. P. Zaletel, and A. Vishwanath, Charged skyrmions and topological origin of superconductivity in magic-angle graphene, Sci. Adv. **7**, eabf5299 (2021).

[43] A. T. Pierce, Y. Xie, J. M. Park, E. Khalaf, S. H. Lee, Y. Cao, D. E. Parker, P. R. Forrester, S. Chen, K. Watanabe *et al.*, Unconventional sequence of correlated Chern insulators in magic-angle twisted bilayer graphene, Nat. Phys. **17**, 1210 (2021).

[44] Y.-D. Liao, X.-Y. Xu, Z.-Y. Meng, and J. Kang, Correlated insulating phases in the twisted bilayer graphene, Chin. Phys. B **30**, 017305 (2021).

[45] A. Rozen, J. M. Park, U. Zondiner, Y. Cao, D. Rodan-Legrain, T. Taniguchi, K. Watanabe, Y. Oreg, A. Stern, E. Berg *et al.*, Entropic evidence for a Pomeranchuk effect in magic-angle graphene, Nature (London) **592**, 214 (2021).

[46] U. Zondiner, A. Rozen, D. Rodan-Legrain, Y. Cao, R. Queiroz, T. Taniguchi, K. Watanabe, Y. Oreg, F. von Oppen, A. Stern *et al.*, Cascade of phase transitions and Dirac revivals in magic-angle graphene, Nature (London) **582**, 203 (2020).

[47] Y. Saito, F. Yang, J. Ge, X. Liu, T. Taniguchi, K. Watanabe, J. Li, E. Berg, and A. F. Young, Isospin Pomeranchuk effect in twisted bilayer graphene, Nature (London) **592**, 220 (2021).

[48] J. M. Park, Y. Cao, K. Watanabe, T. Taniguchi, and P. Jarillo-Herrero, Flavour Hund's coupling, chern gaps and charge diffusivity in Moiré graphene, Nature (London) **592**, 43 (2021).

[49] Y. H. Kwan, Y. Hu, S. H. Simon, and S. A. Parameswaran, Exciton band topology in spontaneous quantum anomalous Hall insulators: Applications to twisted bilayer graphene, Phys. Rev. Lett. **126**, 137601 (2021).

[50] Y. D. Liao, J. Kang, C. N. Breiø, X. Y. Xu, H.-Q. Wu, B. M. Andersen, R. M. Fernandes, and Z. Y. Meng, Correlation-induced insulating topological phases at charge neutrality in twisted bilayer graphene, Phys. Rev. X **11**, 011014 (2021).

[51] J. Kang, B. A. Bernevig, and O. Vafek, Cascades between light and heavy fermions in the normal state of magic-angle twisted bilayer graphene, Phys. Rev. Lett. **127**, 266402 (2021).

[52] J. Liu and X. Dai, Theories for the correlated insulating states and quantum anomalous Hall effect phenomena in twisted bilayer graphene, Phys. Rev. B **103**, 035427 (2021).

[53] F. Schindler, O. Vafek, and B. A. Bernevig, Trions in twisted bilayer graphene, Phys. Rev. B **105**, 155135 (2022).

[54] E. Brillaux, D. Carpentier, A. A. Fedorenko, and L. Savary, Analytical renormalization group approach to competing orders at charge neutrality in twisted bilayer graphene, Phys. Rev. Res. **4**, 033168 (2022).

[55] Z.-D. Song and B. A. Bernevig, Magic-angle twisted bilayer graphene as a topological heavy fermion problem, Phys. Rev. Lett. **129**, 047601 (2022).

[56] J.-X. Lin, Y.-H. Zhang, E. Morissette, Z. Wang, S. Liu, D. Rhodes, K. Watanabe, T. Taniguchi, J. Hone, and J. Li, Spin-orbit–driven ferromagnetism at half Moiré filling in magic-angle twisted bilayer graphene, Science **375**, 437 (2022).

[57] S. Bhowmik, B. Ghawri, N. Leconte, S. Appalakondaiah, M. Pandey, P. S. Mahapatra, D. Lee, K. Watanabe, T. Taniguchi, J. Jung *et al.*, Broken-symmetry states at half-integer band fillings in twisted bilayer graphene, Nat. Phys. **18**, 639 (2022).

[58] T. Huang, X. Tu, C. Shen, B. Zheng, J. Wang, H. Wang, K. Khaliji, S. H. Park, Z. Liu, T. Yang *et al.*, Observation of chiral and slow plasmons in twisted bilayer graphene, Nature (London) **605**, 63 (2022).

[59] S. Zhang, X. Lu, and J. Liu, Correlated insulators, density wave states, and their nonlinear optical response in magic-angle twisted bilayer graphene, Phys. Rev. Lett. **128**, 247402 (2022).

[60] J. Herzog-Arbeitman, A. Chew, D. K. Efetov, and B. A. Bernevig, Reentrant correlated insulators in twisted bilayer

graphene at 25 T (2π flux), Phys. Rev. Lett. **129**, 076401 (2022).
[61] E. Y. Andrei and A. H. MacDonald, Graphene bilayers with a twist, Nat. Mater. **19**, 1265 (2020).
[62] P. Stepanov, M. Xie, T. Taniguchi, K. Watanabe, X. Lu, A. H. MacDonald, B. A. Bernevig, and D. K. Efetov, Competing zero-field Chern insulators in superconducting twisted bilayer graphene, Phys. Rev. Lett. **127**, 197701 (2021).
[63] G. Pan, X. Zhang, H. Lu, H. Li, B.-B. Chen, K. Sun, and Z. Y. Meng, Thermodynamic characteristic for a correlated flat-band system with a quantum anomalous Hall ground state, Phys. Rev. Lett. **130**, 016401 (2023).
[64] X. Zhang, G. Pan, Y. Zhang, J. Kang, and Z. Y. Meng, Momentum space quantum monte carlo on twisted bilayer graphene, Chin. Phys. Lett. **38**, 077305 (2021).
[65] J. S. Hofmann, E. Khalaf, A. Vishwanath, E. Berg, and J. Y. Lee, Fermionic Monte Carlo study of a realistic model of twisted bilayer graphene, Phys. Rev. X **12**, 011061 (2022).
[66] G. Pan, X. Zhang, H. Li, K. Sun, and Z. Y. Meng, Dynamical properties of collective excitations in twisted bilayer graphene, Phys. Rev. B **105**, L121110 (2022).
[67] X. Zhang, G. Pan, X. Y. Xu, and Z. Y. Meng, Fermion sign bounds theory in quantum Monte Carlo simulation, Phys. Rev. B **106**, 035121 (2022).
[68] X. Zhang, K. Sun, H. Li, G. Pan, and Z. Y. Meng, Superconductivity and bosonic fluid emerging from Moiré flat bands, Phys. Rev. B **106**, 184517 (2022).
[69] X. Zhang, G. Pan, B.-B. Chen, H. Li, K. Sun, and Z. Y. Meng, Polynomial sign problem and topological Mott insulator in twisted bilayer graphene, Phys. Rev. B **107**, L241105 (2023).
[70] B.-B. Chen, Y. D. Liao, Z. Chen, O. Vafek, J. Kang, W. Li, and Z. Y. Meng, Realization of topological Mott insulator in a twisted bilayer graphene lattice model, Nat. Commun. **12**, 5480 (2021).
[71] X. Lin, B.-B. Chen, W. Li, Z. Y. Meng, and T. Shi, Exciton proliferation and fate of the topological Mott insulator in a twisted bilayer graphene lattice model, Phys. Rev. Lett. **128**, 157201 (2022).
[72] M. Huang, Z. Wu, X. Zhang, X. Feng, Z. Zhou, S. Wang, Y. Chen, C. Cheng, K. Sun, Z. Y. Meng, and N. Wang, Intrinsic nonlinear Hall effect and gate-switchable Berry curvature sliding in twisted bilayer graphene, Phys. Rev. Lett. **131**, 066301 (2023).
[73] C. Huang, X. Zhang, G. Pan, H. Li, K. Sun, X. Dai, and Z. Meng, Evolution from quantum anomalous Hall insulator to heavy-fermion semimetal in magic-angle twisted bilayer graphene, arXiv:2304.14064.
[74] L. Tagliacozzo, G. Evenbly, and G. Vidal, Simulation of two-dimensional quantum systems using a tree tensor network that exploits the entropic area law, Phys. Rev. B **80**, 235127 (2009).
[75] F. Gliozzi and L. Tagliacozzo, Entanglement entropy and the complex plane of replicas, J. Stat. Mech.: Theory Exp. (2010) P01002.
[76] M. A. Metlitski and T. Grover, Entanglement entropy of Systems with spontaneously broken continuous symmetry, arXiv:1112.5166.
[77] J. D'Emidio, R. Orus, N. Laflorencie, and F. de Juan, Universal features of entanglement entropy in the honeycomb Hubbard model, arXiv:2211.04334.
[78] A. B. Kallin, E. M. Stoudenmire, P. Fendley, R. R. P. Singh, and R. G. Melko, Corner contribution to the entanglement entropy of an $O(3)$ quantum critical point in (2+1) dimensions, J. Stat. Mech.: Theory Exp. (2014) P06009.
[79] Z.-X. Gong, M. Foss-Feig, F. G. S. L. Brandão, and A. V. Gorshkov, Entanglement area laws for long-range interacting systems, Phys. Rev. Lett. **119**, 050501 (2017).
[80] V. Alba, Out-of-equilibrium protocol for Rényi entropies via the Jarzynski equality, Phys. Rev. E **95**, 062132 (2017).
[81] J. D'Emidio, Entanglement entropy from nonequilibrium work, Phys. Rev. Lett. **124**, 110602 (2020).
[82] J. Zhao, B.-B. Chen, Y.-C. Wang, Z. Yan, M. Cheng, and Z. Y. Meng, Measuring Rényi entanglement entropy with high efficiency and precision in quantum Monte Carlo simulations, npj Quantum Mater. **7**, 69 (2022).
[83] J. Zhao, Y.-C. Wang, Z. Yan, M. Cheng, and Z. Y. Meng, Scaling of entanglement entropy at deconfined quantum criticality, Phys. Rev. Lett. **128**, 010601 (2022).
[84] G. Pan, Y. D. Liao, W. Jiang, J. D'Emidio, Y. Qi, and Z. Y. Meng, Stable computation of entanglement entropy for two-dimensional interacting fermion systems, Phys. Rev. B **108**, L081123 (2023).
[85] M. Lohöfer, T. Coletta, D. G. Joshi, F. F. Assaad, M. Vojta, S. Wessel, and F. Mila, Dynamical structure factors and excitation modes of the bilayer Heisenberg model, Phys. Rev. B **92**, 245137 (2015).
[86] Y.-C. Wang, N. Ma, M. Cheng, and Z. Y. Meng, Scaling of the disorder operator at deconfined quantum criticality, SciPost Phys. **13**, 123 (2022).
[87] J. D'Emidio, R. Orus, N. Laflorencie, and F. de Juan, Universal features of entanglement entropy in the honeycomb Hubbard model, arXiv:2211.04334.
[88] Y. Da Liao, G. Pan, W. Jiang, Y. Qi, and Z. Y. Meng, The teaching from entanglement: 2D deconfined quantum critical points are not conformal, arXiv:2302.11742.
[89] Y. Da Liao, Controllable incremental algorithm for entanglement entropy and other observables with exponential variance explosion in many-body systems, arXiv:2307.10602.
[90] See Supplemental Material at http://link.aps.org/supplemental/10.1103/PhysRevB.109.L081114 for the stochastic data collapse scheme that helps accurately determine the critical points and exponents.
[91] K. Fukui and S. Todo, Order-N cluster Monte Carlo method for spin systems with long-range interactions, J. Comput. Phys. **228**, 2629 (2009).
[92] E. J. Flores-Sola, B. Berche, R. Kenna, and M. Weigel, Finite-size scaling above the upper critical dimension in Ising models with long-range interactions, Eur. Phys. J. B **88**, 28 (2015).
[93] J. A. Koziol, A. Langheld, S. C. Kapfer, and K. P. Schmidt, Quantum-critical properties of the long-range transverse-field Ising model from quantum Monte Carlo simulations, Phys. Rev. B **103**, 245135 (2021).
[94] J. Zhao, M. Song, Y. Qi, J. Rong, and Z. Y. Meng, Finite-temperature critical behaviors in 2D long-range quantum Heisenberg model, npj Quantum Mater. **8**, 59 (2023).

[95] B. Berche, R. Kenna, and J.-C. Walter, Hyperscaling above the upper critical dimension, Nucl. Phys. B **865**, 115 (2012).
[96] R. Kenna and B. Berche, A new critical exponent 'coppa' and its logarithmic counterpart 'hat coppa', Condens. Matter Phys. **16**, 23601 (2013).
[97] R. Kenna and B. Berche, Fisher's scaling relation above the upper critical dimension, Europhys. Lett. **105**, 26005 (2014).
[98] E. G. Lazo, M. Heyl, M. Dalmonte, and A. Angelone, Finite-temperature critical behavior of long-range quantum Ising models, SciPost Phys. **11**, 076 (2021).
[99] A. Langheld, J. A. Koziol, P. Adelhardt, S. C. Kapfer, and K. P. Schmidt, Scaling at quantum phase transitions above the upper critical dimension, SciPost Phys. **13**, 088 (2022).
[100] B. Berche, T. Ellis, Y. Holovatch, and R. Kenna, Phase transitions above the upper critical dimension, SciPost Phys. Lect. Notes 60 (2022).
[101] T.-T. Wang and Z. Y. Meng, Quantum monte carlo calculation of critical exponents of the Gross-Neveu-Yukawa on a two-dimensional fermion lattice model, Phys. Rev. B **108**, L121112 (2023).
[102] A. W. Sandvik and D. J. Scalapino, Order-disorder transition in a two-layer quantum antiferromagnet, Phys. Rev. Lett. **72**, 2777 (1994).
[103] M. E. Fisher, S.-k. Ma, and B. G. Nickel, Critical exponents for long-range interactions, Phys. Rev. Lett. **29**, 917 (1972).
[104] We thank Slava Rychkov for clarifying this point.
[105] S. M. Chester, W. Landry, J. Liu, D. Poland, D. Simmons-Duffin, N. Su, and A. Vichi, Bootstrapping Heisenberg magnets and their cubic instability, Phys. Rev. D **104**, 105013 (2021).
[106] T. Kuwahara and K. Saito, Area law of noncritical ground states in 1D long-range interacting systems, Nat. Commun. **11**, 4478 (2020).
[107] M. Song, T.-T. Wang, and Z. Y. Meng, Resummation-based quantum Monte Carlo for entanglement entropy computation, arXiv:2310.01490.
[108] https://cloud.paratera.com.